

Improved Methods for the Registration and Motion Correction of Brain Images

FMRIB Technical Report TR02MJ1

(A related paper has been accepted by Neuroimage)

Mark Jenkinson¹, Peter Bannister^{1,2}, Michael Brady² and Stephen Smith¹

1: Oxford Centre for Functional Magnetic Resonance Imaging of the Brain (FMRIB),

Department of Clinical Neurology, University of Oxford, John Radcliffe Hospital,

Headley Way, Headington, Oxford, UK

2: Medical Vision Laboratory, Department of Engineering Science,

University of Oxford, Oxford, UK

Corresponding author is Mark Jenkinson: mark@fmrib.ox.ac.uk

Abstract

Linear registration and motion correction are important components of structural and functional brain image analysis. Most modern methods optimise some intensity-based cost function to determine the best registration. To date, little attention has been focused on the optimisation method itself, even though the success of most registration methods hinges on the quality of this optimisation. This paper examines the optimisation process in detail and demonstrates that the commonly used multi-resolution local optimisation methods can, and do, get trapped in local minima. To address this problem, two approaches are taken: (1) to apodize the cost function and (2) to employ a novel hybrid global-local optimisation method. This new optimisation method is specifically designed for registering whole brain images. It substantially reduces the likelihood of producing misregistrations due to being trapped by local minima. The increased robustness of the method, compared to other commonly used methods, is demonstrated by a consistency test. In addition, the accuracy of the registration is demonstrated by a series of experiments with motion correction. These motion correction experiments also investigate how the results are affected by different cost functions and interpolation methods.

1 Introduction

Geometric registration and motion correction are important stages in the analysis of functional brain imaging studies. Consequently, it is important that these stages perform robustly and accurately. Furthermore, for large imaging studies it is desirable that they be fully automated.

There has been a considerable amount of research into registration and motion correction of brain images, and many different methods have been proposed [14]. Most methods in common usage are based on the mathematical framework of optimising an intensity-based cost function. However, although much work has concentrated on how the choice of cost function affects registration performance, there has been far less examination of the effect of the optimisation method. Moreover, when optimisation methods are discussed, global methods are often ignored and local methods compared purely on the basis of speed [4].

One of the most common and serious problems for registration methods is the presence of local minima in the cost function. These cause local optimisation methods to “get stuck” and hence to fail to find the desired the global minimum. Most registration methods attempt to solve this problem by incorporating a local optimisation strategy within a multi-resolution framework. Such a multi-resolution framework, which typically involves starting with low resolution images (containing only gross features) and working progressively through to higher resolutions, aims to avoid the local minima “traps”. As we show later, this simple multi-resolution approach is not always sufficient for avoiding local minima, and that by using more sophisticated optimisation methods, the chances of becoming “trapped” in these local minima can be substantially reduced.

Two types of local minima commonly occur for the cost functions used in image registration: large scale basins and small scale dips. The first type, the large scale basin, is responsible for large mis-registrations since the local minimum is often far from the global minimum. The second type, small scale dips, can cause the optimisation to get stuck at any stage and so are responsible for large mis-registrations at low resolutions and for small mis-registrations at high resolutions.

We propose two methods for dealing with the local minima problem. These are: cost function apodization, which reduces or eliminates small scale dips; and a hybrid global-local optimisation technique which utilises prior knowledge about brain registration to create an optimisation technique that combines the speed of local optimisation with the robustness of global optimisation.

The following sections of this paper are: background theory, methods (including both cost function apodization and the hybrid optimisation method), results and discussion. The results section contains a number of experiments on real, whole brain images which demonstrate the effectiveness of the registration in two different settings: (1) structural image registration (inter-modal/inter-subject) of an anatomical image to a standard template; and (2) functional image motion correction (intra-modal/intra-subject) which registers each image in a time-series to a particular example image from that time-series. The first case is examined using a robustness study (as accuracy is hard to define for inter-subject registration, and robustness is a more important issue in this context), while the second case is examined using an accuracy study (as, in this context, it is accuracy that is more important). In each case real brain image data is used. Comparisons with some commonly used methods are also included (in both cases) which demonstrate the superior robustness and accuracy which can be obtained using this approach.

2 Materials

2.1 Registration

The registration problem studied here is to find the best geometric alignment of two (volumetric brain) images. Call the two images the reference (Y) and floating (X) images. More precisely, the registration problem seeks that transformation which, when applied to the floating image, maximises the “similarity” between this transformed floating image and the reference image.

A standard, and common, way of formulating this as a mathematical problem is to construct a cost function which quantifies the dissimilarity between two images, and then search for the transformation (T^*) which gives the minimum cost. In mathematical notation this is:

$$T^* = \arg \min_{T \in S_T} C(Y, T(X)) \quad (1)$$

where S_T is the space of allowable transformations, $C(I_1, I_2)$ is the cost function and $T(X)$ represents the image X after it has been transformed by the transformation T . In this paper we shall only consider linear registration so that S_T is either the set of all affine transformations or some subset of this (such as the set of all rigid-body transformations).

2.2 Cost Function

Many different cost functions have been proposed for image registration problems. Some use geometrically defined features, found within the image, to quantify the (dis)similarity, whilst others work directly with the intensity values in the images. A large comparative study of different registration methods [17] indicated that intensity-based cost functions are more accurate and reliable than the geometrically-based ones. Consequently, most recent registration methods have used intensity-based cost functions, and these are the ones which will be discussed in this paper.

Intensity-based cost functions can be divided naturally into two categories: those suitable for intra-modal problems and those suitable for inter-modal problems. In the former category the most commonly used cost functions are: *least squares* (LS) and *normalised correlation* (NC). For the latter, and more difficult, category the most commonly used functions are: *mutual information* (MI), *normalised mutual information* (NMI), *woods* (W) and *correlation ratio* (CR). These functions are defined mathematically in Table 1 (see [12] for more information).

2.2.1 Interpolation

In addition to a pair of images and a particular transformation, the cost function requires that a method of interpolation be defined. That is, some method of calculating what the intensity is in the floating image at points in between the original voxel (or grid) locations. This is necessary in order to know the intensity at corresponding points in the images after the geometrical transformation has been applied to the floating image.

Interpolation methods that are commonly used are: trilinear (also called linear or, in 2D, bilinear), nearest neighbour, sinc (of various kernel sizes and with or without various windowing functions; e.g. Blackman), spline and Fourier. The choice of method has some impact on cost function smoothness, although all interpolation methods except nearest neighbour are continuous. However, the choice of method becomes most critical for motion correction as the transformed image intensities are needed for later statistical analysis.

2.3 Optimisation

Once a cost function has been chosen it is necessary to search for the transformation which will yield the minimum cost value. To do this, an optimisation method is used which searches through the parameter space of allowable transformations. Note that rigid-body transformations are specified by 6 parameters (3 rotations and 3 translations)

while affine transformations are specified by 12 parameters. Consequently, even for linear transformation, the optimisation takes place in a high dimensional space; \mathcal{R}^n , where $6 \leq n \leq 12$.

While the problem specified in equation 1 is a global optimisation, quite often local optimisation methods are employed as they are simpler and faster.¹ However, this can result in the method returning a transformation that corresponds to a local minimum of the cost function, rather than the desired global minimum. Such cases often appear as mis-registrations, of varying severity, and are a major cause of registration failure.

Unfortunately, there are very few global optimisation methods that are suitable for a 3D brain image registration problem. This is because, in terms of operations, the cost function is expensive to evaluate and most global optimisation methods require a great many evaluations leading to unacceptable execution times (e.g. days).

2.3.1 Multi-Resolution Techniques

To both speed up the optimisation process and to avoid local minima, most currently used registration methods employ some form of multi-resolution optimisation. That is, a sequence of image pairs, at progressively larger spatial scales are created from the initial pair of images: (I^r, I^f) . The images at larger scales are subsampled versions (often with pre-blurring) of the original high-resolution images, and so contain fewer voxels which means that evaluating the cost function requires less computation. In addition, as only gross features of the images remain at these large scales, it is hoped that there will be fewer local minima for the optimisation to “get stuck” in.

2.4 Motion Correction

In functional brain imaging a series of brain images is acquired. The time elapsed between each acquisition is usually a few seconds or less. Due to the small acquisition times required, these images usually have poor resolution. Furthermore, as the imaging parameters are tuned to highlight physiological changes (e.g. blood oxygenation) the images often have poor anatomical contrast.

Extracting functional information from such a series of images is done by applying statistical time-series analysis, which assumes that the location of a given voxel within the brain *does not change over time*. However, there is

¹A *global* method searches the entire range of possible parameters for the most optimal cost function value, whilst a *local* method simply starts somewhere in parameter space and moves about locally trying to find an optimum, and stopping when there is no better nearby set of parameters.

usually some degree of subject motion within the scanner, especially when the scanning takes a long time or when clinical patients are involved. Therefore, in order to render the data fit for statistical analysis this motion must be estimated and corrected for. This is the task of motion correction methods and it is essentially a multiple-image registration task.

Normally motion correction methods deal with the registration task by selecting a reference image from within the series and registering each image in turn to this fixed reference. As all images are of the same subject, using the same imaging parameters, it can be classified an intra-subject, intra-modal registration problem. Therefore, a rigid-body transformation space and intra-modal cost function can be used. Furthermore, as the values in the corrected images are important for later statistical analysis, the choice of interpolation method for the transformation of the images is of particular importance (Hajnal et al.,1995a, b).

3 Methods

3.1 Apodization of the Cost Functions

As seen in Figure 1, the local behaviour of the cost function shows small discontinuities as the transformation parameters are varied smoothly. This creates local minima “traps” for the optimisation method. Since all interpolation methods are continuous (except nearest neighbour which is consequently seldom used) the discontinuities are not due to the type of interpolation used. The cause of these discontinuities is the changing amount of overlap of the reference and floating image.

There are two different ways of treating values outside the Field of View (FOV) of an image:

1. Treat all values outside the FOV as zero.
2. Do all calculations strictly in the overlapping region.

The first method is undesirable as it creates artificial intensity boundaries when the object is not wholly contained within the FOV. However, in the second method the number of points counted in the overlapping region varies, not just the expressions involving intensities. Therefore, in the second case both the numerator and denominator of the cost functions (except Least Squares) will change discontinuously as the amount of overlap changes.

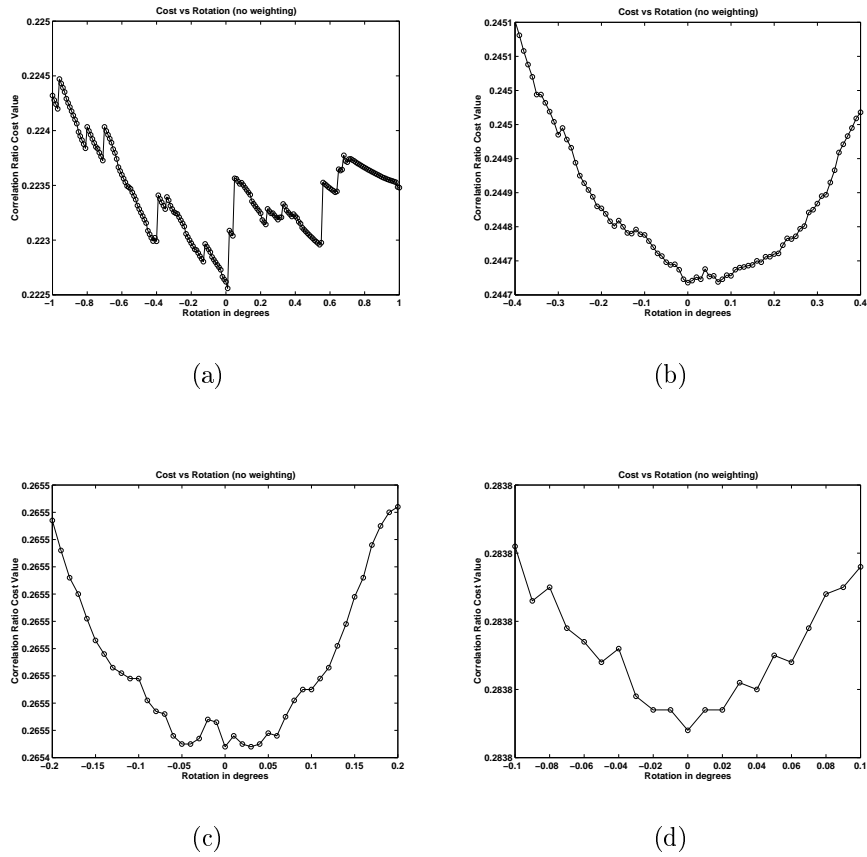


Figure 1: Plots of the Correlation Ratio cost function versus rotation about the x -axis, showing the presence of local discontinuities. Such discontinuities can sometimes signify the presence of local minima. The resolution of the images are: (a) 8mm, (b) 4mm, (c) 2mm and (d) 1mm. Note that the range of angles shown and the size of discontinuity decreases as the resolution scale decreases. Therefore the problem is greater at larger scales. Note that each individual sample of the cost function is denoted by a circle.

The discontinuities exist because the images are discrete sets of voxels. In particular, the reference image defines a fixed set of voxel locations over which the cost function is calculated. Then, for a given transformation, the floating image intensities at these locations are calculated using interpolation. A reference image voxel location is only counted when it is valid: that is, within the overlapping region such that it maps to a location inside the FOV of the floating image. When the edge of the FOV of the floating image crosses a reference voxel location, the location suddenly goes from being inside the overlapping region to outside, causing a discontinuous change in the number of valid locations, as shown in Figure 2.

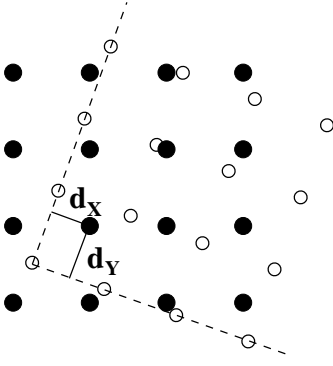


Figure 2: Example showing how the overlapping region of the FOV for the reference image (filled dots) and floating image (open dots) can change with transformation. The shortest distances, d_X and d_Y , (shown as a solid lines) to the edges of the overlapping region (shown by the dashed lines) are illustrated for a single reference voxel location.

We aim to apodize the cost function by removing these discontinuities. To do this, our approach has been to introduce a geometric apodization that de-weights the contributions of locations that are near the edge of the overlapping region. The weighting is chosen so that the contribution of such locations drops continuously until it reaches zero at the edge of the overlapping region. Any continuous weighting function could be used but for simplicity and computational efficiency we choose one that is linear.

For instance, consider a 2D example of a reference location that maps to a point inside the overlapping region, where the distance from the nearest edges of the floating image FOV are d_X and d_Y units, as shown in Figure 2. In each dimension, if this value is less than some threshold D , then the influence of that point is weighted by a weight $w = d/D$. In higher dimensions, the product of the weighting functions in each dimension is used. That is:

$$w(d_X, d_Y, d_Z) = w(d_X)w(d_Y)w(d_Z).$$

The weighting is applied to all terms involving that location's intensity as well as to the number of locations in the region. For example, consider the n th moment of an iso-set:

$$M_n\{Y_k\} = \frac{1}{N_k} \sum_{j|X_j \in I_k} (Y_j)^n \quad (2)$$

$$N_k = \sum_{j|X_j \in I_k} 1. \quad (3)$$

where M_n is the n th moment, j is a voxel index, X and Y represent the reference and floating images respectively

and I_k denotes the k th intensity bin. With general weighting this becomes:

$$M_n\{Y_k\} = \frac{1}{N_k} \sum_{j|X_j \in I_k} w_j (Y_j)^n \quad (4)$$

$$N_k = \sum_{j|X_j \in I_k} w_j. \quad (5)$$

where w_j is the weight of the location j , which is 0 outside the overlapping region, d/D for $d < D$ or 1 for $d \geq D$ inside the overlapping region.

This weighting scheme can be simply and efficiently applied to any of the non entropy-based cost functions (i.e. LS, NC, W and CR). It depends on one parameter — the threshold distance D — which can be varied to increase the amount of apodization. When $D = 0$ there is no apodization, whilst increasing D creates smoother and smoother cost functions, although the cost function will be continuous for *any* non-zero value of D . Also note that making D larger than the voxel spacing is permitted and just has a greater smoothing effect, as shown in Figure 3.

3.1.1 Joint Histogram Apodization

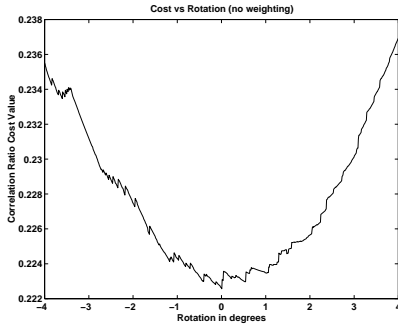
A more general weighting scheme is required for apodizing the joint histogram required for the entropy-based cost functions. This is because the number of entries in each histogram bin becomes discontinuous as the intensity at a floating image location (calculated using interpolation) passes through the threshold value between intensity bins.

As it is the intensity passing through a threshold value that causes the discontinuities for the joint histogram, we propose a weighting function that is determined by the intensities and applied to every location. We choose, once again, a linear weighting function (as shown in Figure 4) where w_k is the weight for bin k , I is the intensity at the location under consideration, T_k is the intensity threshold between bins $k - 1$ and k , and Δ is the smoothing threshold — the equivalent of D in the preceding section. This weight is then applied to the accumulation of intensity within the joint histogram bin, as well as the number of entries in the bin, which is no longer an integer. That is for a point of intensity I , the updating equations for bin k are:

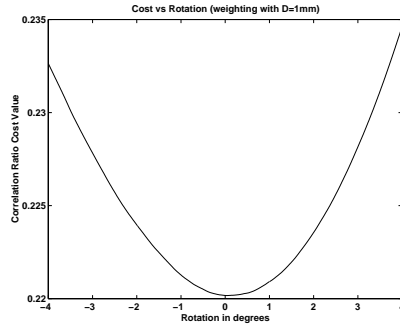
$$N_k \rightarrow N_k + w_k(I)$$

$$S_k \rightarrow S_k + I \cdot w_k(I)$$

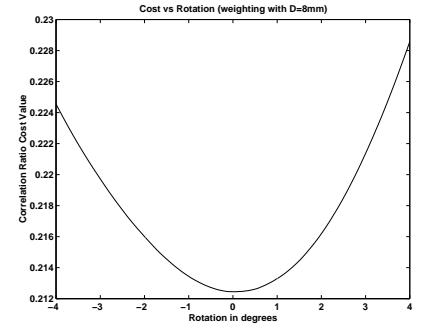
where $w_k(\cdot)$ is the weighting function for the k th bin (see figure 4), N_k is the occupancy of bin k (a non-integer version of the number of elements), and S_k is the sum of intensities in the bin.



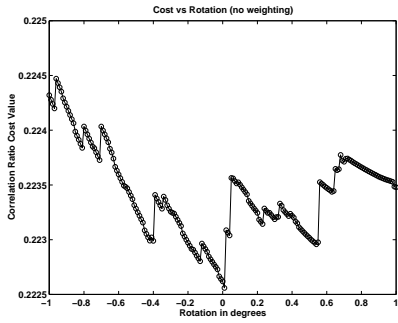
(a)



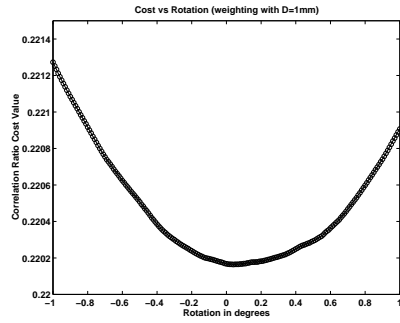
(b)



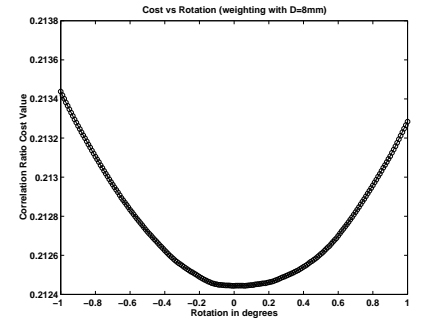
(c)



(d)



(e)



(f)

Figure 3: Plots of the Correlation Ratio cost function versus rotation at different values for the geometric apodization threshold, D . The values of D shown are 0mm, 1mm and 8mm for the three columns (left to right respectively). The resolution in each case is 8mm and the bottom row shows the same values over an expanded scale. Each plot was generated by measuring the cost functions between two real images, about the estimate of the global minimum, which was a non-identity transformation and so did not correspond to maximum overlap of the FOVs. This clearly shows that the apodization has the desired smoothing effect on the cost function, eliminating large discontinuities. Note that each individual sample of the cost function in the bottom row is denoted by a circle.

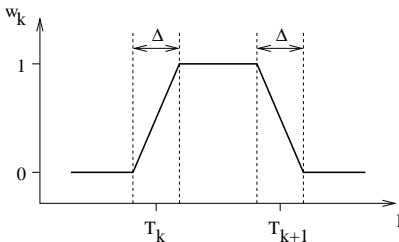


Figure 4: Weighting function used for apodization of the entropy-based cost functions. This weighting function is equivalent to a fuzzy-bin membership function based on the intensity I .

This approach is effectively fuzzy-binning, where each intensity bin no longer has sharp thresholds, but fuzzy membership functions. It also means that a given location can influence more than one bin entry. Because of the way the weighting function is calculated though, each location contributes equally, since the sum of weights for all bin entries is equal to one.

As changing overlap will still create discontinuities, both the geometrical weighting and the fuzzy-binning need to be applied to have a continuous joint histogram. Moreover, the parameter Δ will give a continuous joint histogram for any value greater than zero, although the value should not exceed the intensity bin width. The smoothing capacity of Δ is shown in Figure 5 for the Mutual Information cost function. Results for the Normalised Mutual Information cost function are very similar. Note that, in general, a value of $\Delta = 0.5$ together with D equal to the resolution scale (e.g. 8mm), gives a desirably smooth cost function.

Note that the Partial Volume Interpolation introduced by Maes [13] also creates continuous joint histogram estimates if used in conjunction with the geometrical weighting (applied to the reference locations instead). However, as the name suggests, PVI is more than just a apodization scheme — in fact it functions as an interpolation method too. Therefore, different interpolation methods cannot be used in conjunction with PVI, whereas for fuzzy-binning the interpolation method used can be freely chosen. Furthermore, the fuzzy-binning scheme provides an adjustable parameter, Δ , which controls the amount of smoothing of the cost function, allowing for different degrees of smoothing, as desired.

Finally, it can be seen that fuzzy-binning can be made fully symmetric with respect to the two images (see [2] for a discussion of symmetry in general registration cost functions). That is, both floating and reference intensities can have fuzzy-binning applied to them. However, there is an inherent asymmetry in the way that interpolation is

applied only to the floating image. Therefore, although such a symmetric approach appears initially attractive, the simpler and faster approach of only using fuzzy-bins for the floating image was adopted in practice.

3.2 A Global-Local Hybrid Optimisation Method

Of the many different approaches to global optimisation we have investigated two strategies and combined them with a simple but fast local optimisation method to produce a hybrid optimisation method. The two strategies are: searching and multi-start optimisation.

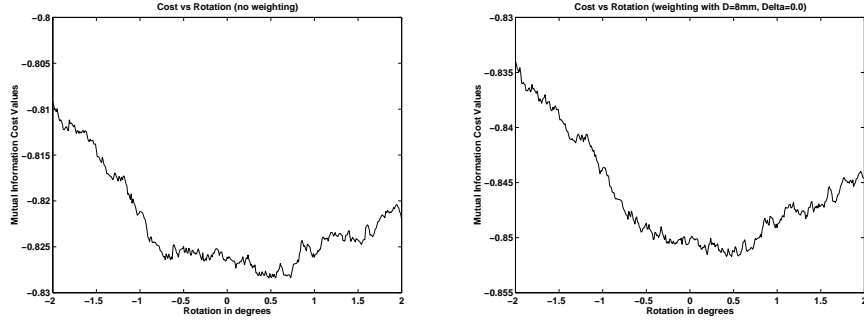
Our hybrid optimisation method (also described in [12]) is specifically designed for the problem at hand, using prior knowledge about the transformation parameters and typical data size (FOV, voxel size, etc.) to help make the method efficient. The method cannot guarantee that the global solution is found, but then neither can any other global optimisation method given a finite amount of time. Generally, only statistical “guarantees” are given, and these often require excessive run-times in order to be met. In contrast, our method is designed to give a reliable estimate of the global minimum given some time restriction (in our case, less than one hour on a moderately-powered standard workstation; e.g. registering two $1 \times 1 \times 1$ mm images typically takes 15 minutes on a 500MHz Pentium III).

The method still uses a local optimisation method with a multi-resolution framework, and these are described in the next two sections, followed by descriptions of the global search and multi-start optimisation strategies employed.

3.2.1 Multi-Resolution

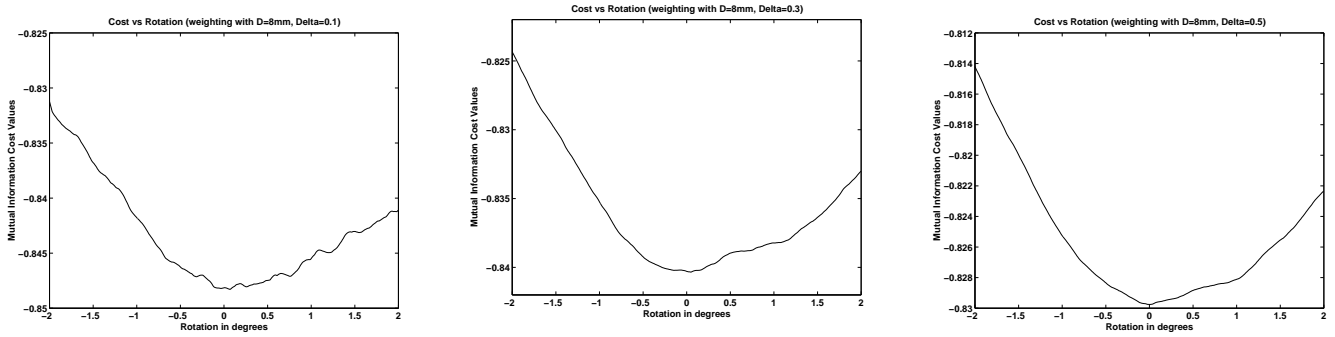
Currently, four different scales are used in our method: 8mm, 4mm, 2mm, 1mm. At each scale, the two images are resampled, after initial pre-blurring (using a Gaussian with FWHM equal to the ratio of the final and initial voxel sizes), so that they have isotropic voxels of size equal to the scale size. Note that an exception to this occurs if the scale is smaller than the data resolution, in which case the data is resampled to isotropic voxels of scale closest to the data resolution.

Furthermore, skew and anisotropic scaling changes are much less prominent than rotational, translational and global scaling changes and so their effects are difficult to estimate reliably at low resolutions. Consequently, only similarity transformations (rigid-body + global scaling) are estimated at the 8mm and 4mm scales.



(a)

(b)



(c)

(d)

(e)

Figure 5: Plots of the Mutual Information cost functions versus rotation at different values for the fuzzy-binning apodization threshold, Δ . The values of Δ shown are 0.0 for the top row and 0.1, 0.3 and 0.5 for the three columns (left to right respectively) in the bottom row. In (a) no geometric apodization is applied, whilst in (b) to (e), the geometric apodization with $D = 8\text{mm}$ is applied together with fuzzy-binning for (c) to (e). The resolution of the image in each case is 8mm. Each plot was generated by measuring the cost functions between two real images, about the estimate of the global minimum, which was a non-identity transformation and so did not correspond to maximum overlap of the FOVs. This clearly shows that both apodization methods are required to have the desired smoothing effect on the cost function, eliminating large discontinuities. In general, a value of $\Delta = 0.5$ together with D equal to the resolution scale (e.g. 8mm), gives a desirably smooth cost function.

3.2.2 Local Optimisation

The choice of local optimisation method used here is not critical, except that it must be efficient. Furthermore, since it will be used in a multi-resolution framework, the low resolution stages do not need to find highly accurate transformations. Therefore the initial parameter bracketing and the parameter tolerances (the size of uncertainty on the optimised parameter values) are both made proportional to the scale size. This avoids many unnecessary cost function evaluations at low resolutions.

We initially chose Powell’s method [15] as our local optimisation method as it was efficient and did not require gradients to be calculated which are especially difficult given the apodizations applied to the cost functions. However, we discovered that a set of N 1D golden searches [15] gave equally good results, which can be reasonably expected if the parameterisation is close to decoupled.

3.2.3 Global Search

To estimate the final transformation sufficiently accurately, a brute-force search of the transformation space is infeasible, even for rigid-body transformations. However, at the lowest resolution (8mm scale) only the gross image features still exist and so a coarse search of the cost function at this resolution should reflect the major changes in rotation, translation and global scaling, allowing large mis-registrations to be avoided.

Speed remains an issue, even for coarse searches at low resolution. Therefore, the search is restricted to the rotation parameters, as these are the most difficult to find and are the cause of many large mis-registrations. Furthermore, the search is divided into three stages:

1. a coarse search over the rotation parameters with a full local optimisation of translation and global scale for each rotation tried;
2. a finer search over rotation parameters, but with only a single cost function evaluation at each rotation (for efficiency);
3. a full local optimisation (rotation, translation and global scale) for each local minimum detected from the previous stage.

The first of these stages is straightforward. Given a set of rotations to try (by default we use 60° increments

in each of the Euler angles, leading to $6^3 = 216$ different rotations), the local optimisation routine is called for the translation and global scale only. That is, the rotation is left fixed, and the best translation and global scale for this particular rotation is found. These results are then stored for use in the later stages.

The second stage takes a larger set of rotations (by default we use 18° degree increments, leading to $20^3 = 8000$ different rotations) but only evaluates the cost function once for each rotation. This contrasts with the previous stage where the cost function is typically evaluated between 10 and 30 times during the local optimisation. However, in order for the evaluation to be a reasonable estimate of the best cost function with this rotation, the translation and global scale parameters must be close to the optimal values. These parameter values are supplied from the results of the previous stage, with the translation parameters determined by interpolating between the stored translation values. Global scale is fixed at the median global scale value over all the stored values. This is done differently from the translation as the scale should not vary greatly with rotation, whereas the translation is highly coupled with the rotation values.

Finally, the third stage applies a full local optimisation, allowing rotation to vary, at each local minimum detected from the results of the previous stage. These local minima are defined as rotations where the cost value found is less than for any of the “neighbouring” rotation values. There are often several such local minima, and rather than force the selection of the best one at this stage, they are all optimised and passed onto the higher resolution stages.

Although it is unlikely that the first stage in this process will get very close to the correct rotation, the second stage should get close enough for the local optimisation in the last stage to give a good estimate. Note that in most registration methods there is no equivalent of this search and a single local optimisation is performed with the starting point being no rotation, no translation and unity scaling (the identity transformation). As this method examines many more possible starting transformations, cannot do any worse than these simple methods.

3.2.4 Multi-Start Optimisation with Perturbations

Following the previous search stage (at 8mm scale) there are usually several local minima selected as candidates for initialising more detailed searches for the global minimum. This stage (at 4mm scale) performs a local optimisation for the best of these candidate transformations. In addition, it takes several perturbations of the candidate transformations and performs local optimisation of these perturbations. Finally, the single best (minimum cost)

solution is selected from among these optimisation results.

In practice, the three best candidates are taken from the previous stage, together with ten perturbations of each candidate. Two perturbations are applied to each rotation parameter, each being half the magnitude of the fine search step size from the previous stage. As well as these six rotational perturbations, four perturbations in scale ($\pm 0.1, \pm 0.2$) are also applied. The number and size of the perturbations used is arbitrary, with these values chosen here being selected largely from experience with the magnitude and type of typical mis-registrations.

This approach of trying several candidate solutions is effectively a multi-start strategy similar to that used in genetic algorithms and other global optimisation methods. Furthermore, the use of “local” perturbations is similar to the way in which alternatives are generated in simulated annealing. It has been found empirically that the combination of these strategies, together with the initial search, avoids getting trapped in local minima to a much greater extent than for a local optimisation method alone within a multi-resolution framework.

3.2.5 Higher Resolution Stages

Following the 4mm scale the single best candidate transformation is chosen, and it is only this transformation which is worked with from here on. At the 2mm scale the skews and anisotropic scalings start to become significant. Consequently, these extra Degrees of Freedom (DOF) are progressively introduced by calling the local optimisation method three times: first using only 7 DOF (rigid-body + global scale), then with 9 DOF (rigid-body + independent scalings), then with the full 12 DOF (rigid-body + scales + skews).

Since the cost function evaluations take 8 times longer at the 1mm scale than at the 2mm scale, and 512 times longer than at the 8mm scale, only a single pass of the local optimisation is done at the 1mm scale. The result of this single pass is returned as the registration solution, T^* .

3.3 Motion Correction

In broad terms, a motion correction algorithm must take a time series of fMRI images and register each image in the series to a reference image. This reference image may be of a different modality [1] but a more common approach is to select one image from the time-series itself (usually the first — c.f. SPM [7]) and register the remaining images to this template image.

If we make the reasonable assumption that there is unlikely to be large motion from one image to the next (usually 3 seconds between images or less), we can use the result of one image’s registration as an initial guess for the next image in the series. This is accomplished by assuming an initial identity transformation between the middle image V_n in a time series and the next adjacent image V_{n+1} and then finding the optimal transformation T_1 by optimising the cost function. The resulting solution is then used as a starting point for the next optimisation with the next image pair V_n, V_{n+2} (see Figure 6). This is only done at the lowest resolution, as all higher resolutions use the transformations found at the next lower resolution for the initial estimates.

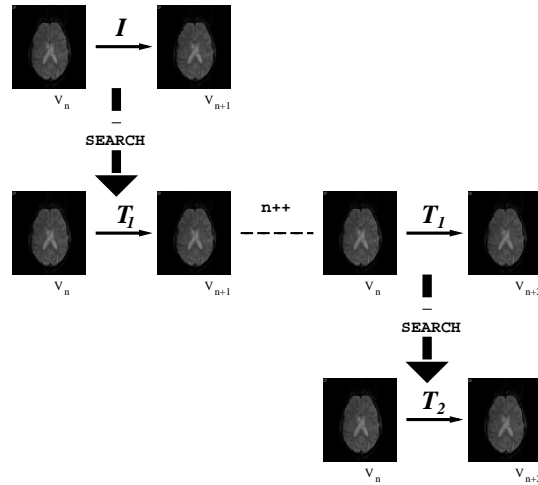


Figure 6: Schematic of the rigid-body motion correction scheme. The median indexed image of the series (V_n) is regarded as the reference image and each transformation (T_1) to an adjacent image is used as the initial ‘guess’ for the transformation between that image and the one beyond (V_{n+1} ; $n++$ signifies an increment of n).

The final schedule carries out the following steps on the uncorrected data (optional stages are shown in *italics*):

- 8mm optimisation using the middle image as initial reference and then using each result to initialise next pairwise optimisation
- 4mm optimisation using middle image as reference and 8mm stage results as initialisation parameters
- 4mm optimisation (lower tolerance) using middle image as reference and 4mm stage results as initialisation parameters
- Mean Registration option:

- *Apply transformation parameters from high tolerance 4mm stage*
 - *Average corrected images to generate mean template image*
 - *Carry out 8mm, 4mm and 4mm (high tolerance) optimisations as before but against mean image as reference.*
- Sinc Registration option:
 - *Carry out additional 4mm (high tolerance) optimisation using sinc interpolation (instead of trilinear as used in previous stages)*
 - Apply current transformation parameters to uncorrected data and save

3.3.1 End Slices

As the intensity values are of great interest after motion correction, attention must be paid to not only the estimation but the application of the transformation. Interpolation probably has the largest impact on the quality of the transformed data, with sinc interpolation methods often being used, although no absolute consensus on the best method exists. However, the loss of information outside the FOV, usually seen in the end slices, can also be very detrimental to the final statistical maps in these areas.

Our motion correction implementation has also been designed to handle the potentially problematic issue of end-slice interpolation. It is frequently the case that under even small affine motion of the head, voxels in the top and bottom slices can move either in or out of the field of view (see Figure 7). Other schemes approach this by either assuming that all affected voxels are zero (AIR) or can be completely excluded from further calculations (SPM). This clearly impacts later analysis as valuable spatial information may be lost.

We counter this situation by padding the end-slices when applying the estimated transformation (i.e. increasing the extent of each volume by 2 slices). This means that if data is to be interpolated from outside the FOV, it will take on 'sensible' values (Personal Communication with Roger Woods, 1999).

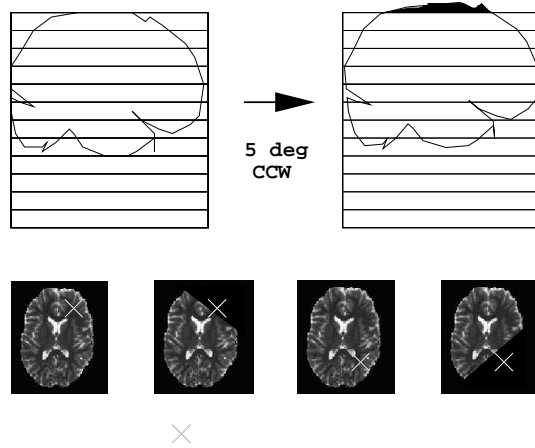


Figure 7: Top row: demonstration of a significant section of brain moving out of the FOV (depicted as a stacked-slice grid) when the patient exhibits 5° pitch about the center of the brain. Bottom row: Corresponding voxels in adjacent scans (shown as white crosses) can be lost if there is appreciable movement of brain in the end slices. Diagram shows reference brain and corrected slice which has moved out of the FOV because of patient motion for two movements

4 Results

This section presents several experiments that demonstrate the robustness and accuracy of the proposed registration and motion correction method. We begin by first stating the implementational choices made as these are often critical in creating a stable method that performs well. Following this the experiments for registration are presented which clearly demonstrate the improved robustness, with the following sections on motion correction and atrophy estimation, demonstrating the improved accuracy.

4.1 Implementation: FLIRT and MCFLIRT

The registration and motion correction methods described in the previous sections have been implemented in C++ and are called FLIRT (FMRIB's² Linear Image Registration Tool) and MCFLIRT (Motion Correction FLIRT). In each case several implementation choices needed to be made to obtain a robust, working method. The more important choices are: (1) the use of Centre of Mass as the centre of transformation (also used for initial alignment);

²The Oxford Centre for Functional MRI of the Brain.

(2) the parameterisation of the transformations as three Euler angles, three translations, three scales and three skews; and (3) the number of intensity histogram bins set to 256 *divided by the scale size* (i.e. 256 for 1mm scaling but only 32 for 8mm scaling) since the number of voxels (samples) is small for large scalings and so fewer bins must be used in order to get reliable statistics [10]. Each of these choices is detailed more fully in [12].

4.2 Robustness Assessment: Registration

4.2.1 Consistency Test

For many registration problems in practice, there is no ground truth available to evaluate the registration. This makes the quantitative assessment of methods quite difficult. Therefore, to test the method quantitatively, a comparative consistency test was performed that does not require knowledge of the actual ground truth.

The consistency test is based on comparing registrations obtained using various different, but known, initial starting positions of a given image. If the registrations are consistent then the final registered image will be the same, regardless of the starting position. Consistency is a *necessary, but not sufficient* condition that all correctly functioning registration methods must possess. This is essentially a measure of the robustness rather than the accuracy [17] of the registration method. Robustness is defined here as the ability to get close to the global minimum on all trials, whereas accuracy is the ability to precisely locate a (possibly local) minimum of the cost function. Ideally a registration method should be both robust and accurate.

More specifically, the consistency test for an individual image I involved taking the image and applying several pre-determined affine transformations, A_j to it (with appropriate cropping so that no ‘padding’ of the images was required). All these images (both transformed and un-transformed) were registered to a given reference image, I^r , giving transformations T_j . If the method was consistent the composite transformations $T_j \circ A_j$ should all be the same, as illustrated in Figure 8.

The transformations are compared quantitatively using the RMS deviation between the composite registration $T_j \circ A_j$ and the registration from the un-transformed case T_0 . This RMS deviation is calculated directly from the affine matrices [11]. That is:

$$d_{RMS} = \sqrt{\frac{1}{5}R^2 \text{Tr}(M^\top M) + t^\top t}, \quad (6)$$

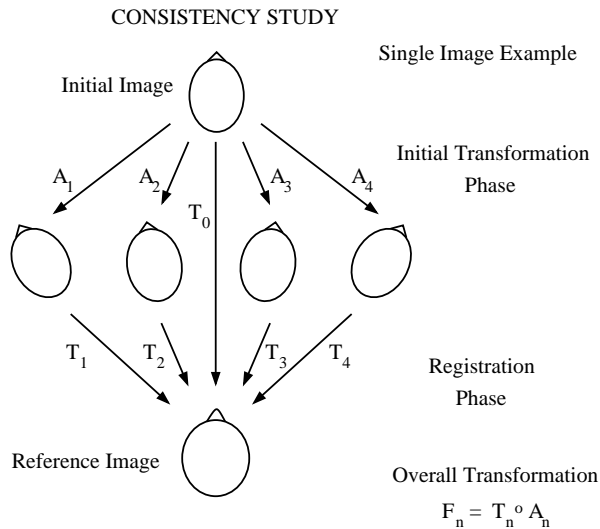


Figure 8: Illustration of the consistency test for a single image. An image (top) has a number of initial affine transformations A_j applied to it. The resulting images (middle) are then registered to the reference image (bottom), giving transformations T_j . Therefore, the overall transformation from the initial image to the reference image is $F_j = T_j \circ A_j$, and these are compared with T_0 which is the registration of the initial image directly to the reference image. For a consistent method, all the transformations, F_j , should be the same as T_0 .

where d_{RMS} is the RMS deviation in mm, R is a radius specifying the volume of interest, and $\begin{pmatrix} M & t \\ 0 & 0 \end{pmatrix} = T_j \cdot A_j \cdot T_0^{-1} - I$ is used to calculate the 3×3 matrix M and the 3×1 vector t .

4.2.2 Comparison with Existing Methods

A comparison of FLIRT with several other registration packages was initially performed using the consistency test explained above. The other registration packages used were AIR [19], SPM [6], UMDS [16] and MRITOTAL [3]. These methods were chosen because the authors' implementations were available, and so this constituted a fair test as opposed to a re-implementation of a method described in a paper, where often the lack of precise implementation details makes it difficult to produce a good working method.

The particular experiment that was performed was *inter-subject* and *inter-modal* using 18 different images as the floating images (like the one shown in Figure 9), all with the MNI 305 brain [3] as the reference image. The 18 images were all $256 \times 256 \times 30$, T2-weighted MR images with voxel dimensions of 0.93mm by 0.93 mm by 5mm,

while the MNI 305 template is a $172 \times 220 \times 156$, T1-weighted MR image with voxel dimensions of 1mm by 1 mm by 1mm.

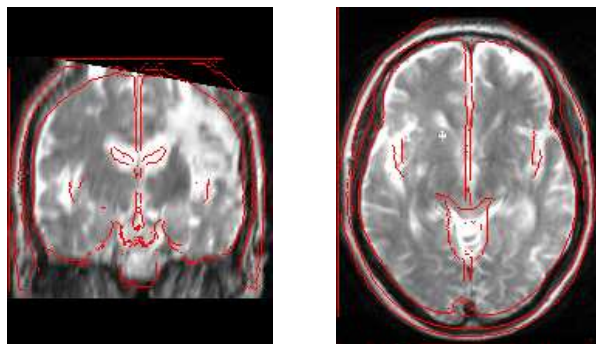


Figure 9: Example slices from one of the images used in the consistency study (after registration). The red lines represent edges from the standard image (the reference image) overlaid on the transformed initial image.

The results of one such test, using six different rotations about the Anterior-Posterior axis, are shown in Figure 10. It can be seen that only FLIRT and MRITOTAL performed consistently. This indicates that the other methods (AIR, SPM and UMDS) frequently get trapped in local minima, i.e. are not as robust.

A further consistency test was then performed comparing only MRITOTAL and FLIRT. This test used initial scalings rather than rotations. The reason that this is important is that MRITOTAL uses a multi-resolution local optimisation method (Gradient Descent) but relies on initial pre-processing to provide a good starting position. This pre-processing is done by finding the principle axes of both images and initially aligning them. Consequently the initial alignment compensates for rotations but does not give any information, and hence correction, for scalings.

The results of the scaling consistency test are shown in Figure 11. It can be seen that, although generally consistent, in three cases MRITOTAL produces registrations that deviate by more than 20mm (RMS) from each other. In contrast, FLIRT was consistent (less than 2mm RMS) in all cases.

4.3 Accuracy Assessment: Motion Correction

This section details the comparative accuracy of the Motion Correction scheme (MCFLIRT) when tested against two of the most widely-used schemes: SPM and AIR.

In order to attempt to establish a “gold standard” for registration accuracy, initial tests use the RMS measure

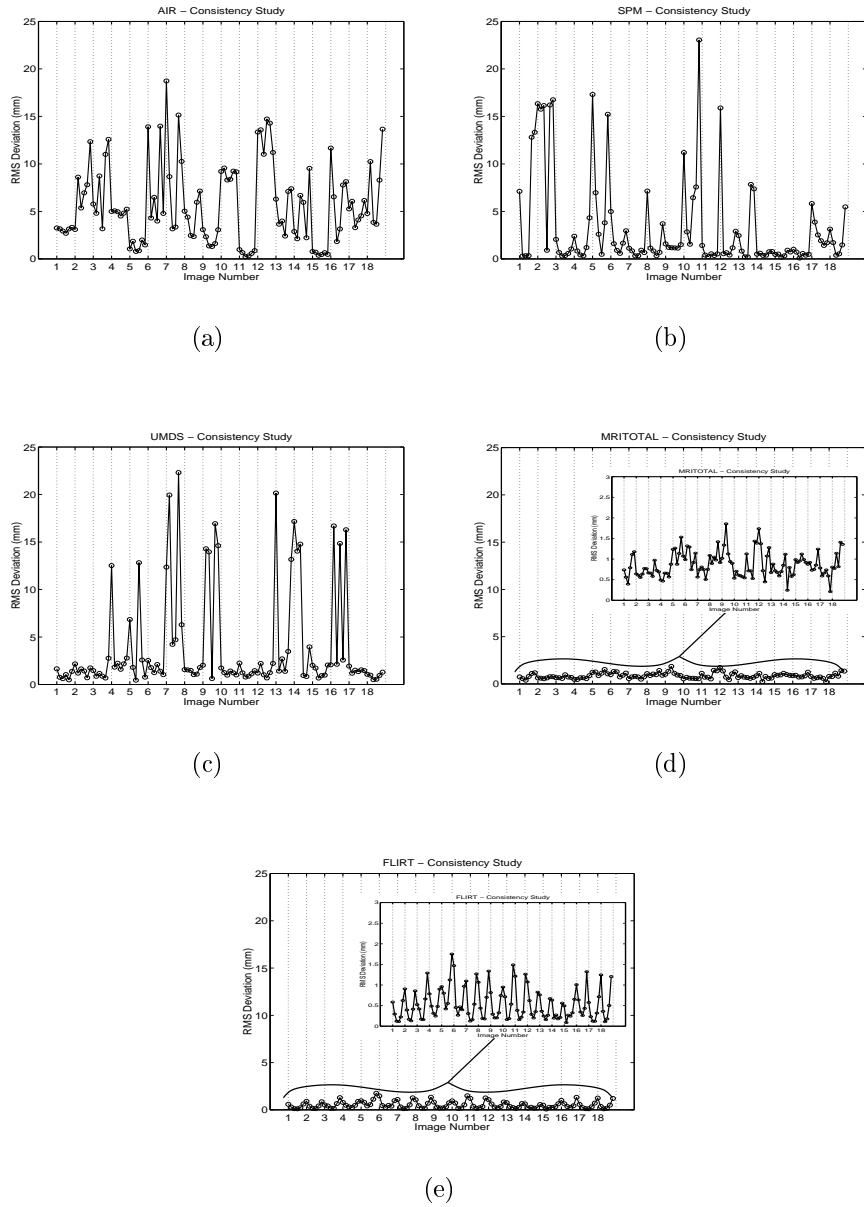


Figure 10: Results of the consistency study, plotting RMS deviation (in mm) versus image number for (a) AIR, (b) SPM, (c) UMDS, (d) MRITOTAL and (e) FLIRT. For each of the 18 source images (T2-weighted MRI images with voxel dimensions of 0.93mm by 0.93 mm by 5mm) there are 6 results corresponding to initial starting rotations of -10,-2,-0.5,0.5,2, and 10 degrees about the y -axis (anterior-posterior axis). All of the methods, except FLIRT and MRITOTAL, show large deviations and are therefore inconsistent and non-robust.

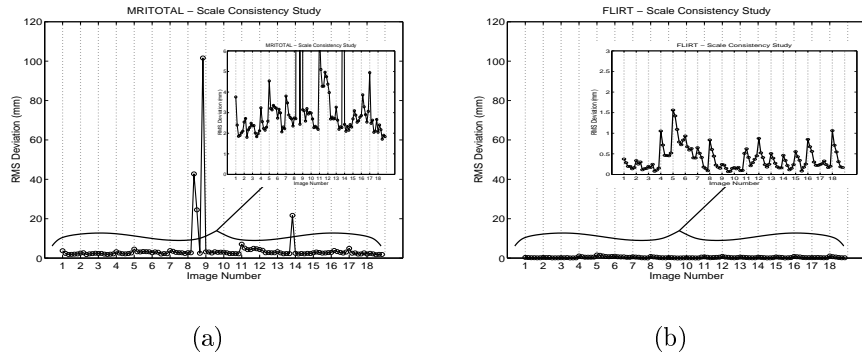


Figure 11: Results of the scale consistency study, plotting RMS deviation (in mm) versus image number for (a) MRITOTAL and (b) FLIRT. For each of the 18 source images (T2-weighted MRI images with voxel dimensions of 0.93mm by 0.93 mm by 5mm) there are 6 results corresponding to initial scalings of 0.7, 0.8, 0.9, 1.1, 1.2 and 1.3 about the Centre of Mass. In three cases MRITOTAL shows large deviations and so is less consistent and robust than FLIRT in this case.

(equation 6) in combination with synthetic data, where the exact value of the motion is known, in order to quantify the scheme’s ability to correct for subject motion. Later tests characterise the degree of correction by examining the residual variation (collapsed across time) in the corrected data. This measure is also used to test the scheme’s effectiveness on real data where we have no absolute measure of the subject’s movement.

4.3.1 Simulated Data

The artificial data enabling gold standard comparisons were generated as follows: a high resolution EPI volume (2 x 2 x 2 mm) was duplicated 180 times and each volume was transformed by an affine matrix corresponding to real motion estimates taken from one of two studies where the subject had been asked to move their head appreciably during the scan. Three further groups of images were generated using motion estimates from experiments where the subject had been asked to remain as still as possible. Within these five motion designs, three further groups of data were created corresponding to audiovisual activation at 0%, 2.5% and 5% of the overall voxel intensities by modulating the intensity values according to a mask derived from real fMRI data. Once the activation (if any) had been applied and the volumes transformed by the corresponding parameters, the data was subsampled to 4mm x 4mm x 6mm voxels, and appropriately cropped to avoid introducing any ‘padding’ voxels. The use of a high resolution template image which is then subsampled should minimise the effect of interpolation when applying such

transformations to the data.

Within our correction scheme, there are a number of stages which can be tuned to optimise the accuracy of the correction. The remainder of this section aims to find a robust set of parameters which give consistently accurate results on all data presented. We begin by examining the comparative accuracy of several cost functions which can be used with our optimisation scheme. Later we proceed to examine the impact made by the choice of interpolation scheme and registration schedule.

4.3.2 Cost Functions

The test results shown in Figure 12 show the relative accuracy of the available cost functions within the MCFLIRT optimisation framework when applied to the problem of motion correction on our synthetic data.

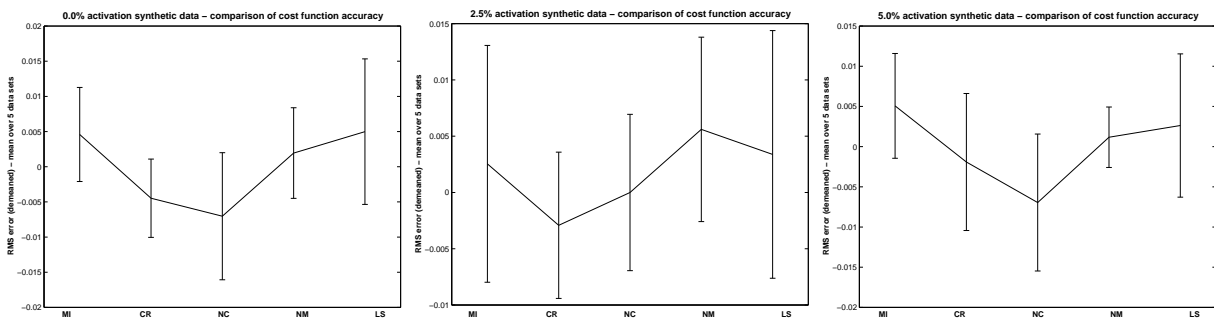


Figure 12: Median (over time) RMS (over space) error results for the MCFLIRT scheme applied to synthetic data exhibiting known motion of one of five designs and audiovisual activation at increasing intensities. Cost function notation corresponds to Table 1

Although there is no clear leader over all cost functions in terms of accuracy, we note that the most accurate results are predominantly yielded by the Normalized Correlation and Correlation Ratio cost functions. This observation is reinforced when we examine the number of data sets where a particular cost function is most accurate. This is summarised in Table 2.

Note that previous work [5] which had demonstrated the superiority of entropy-based cost measures over alternatives in terms of motion correction without introducing further spurious activations in the data, has only compared Mutual Information metrics against least squares (SPM) and Woods (AIR) measures.

The next stage of testing was to verify that these cost functions were in fact more accurate when smoothed

(apodized) than un-smoothed (un-apodized). The same RMS test measure and data sets were used as in the previous test and results are given in Figure 13.

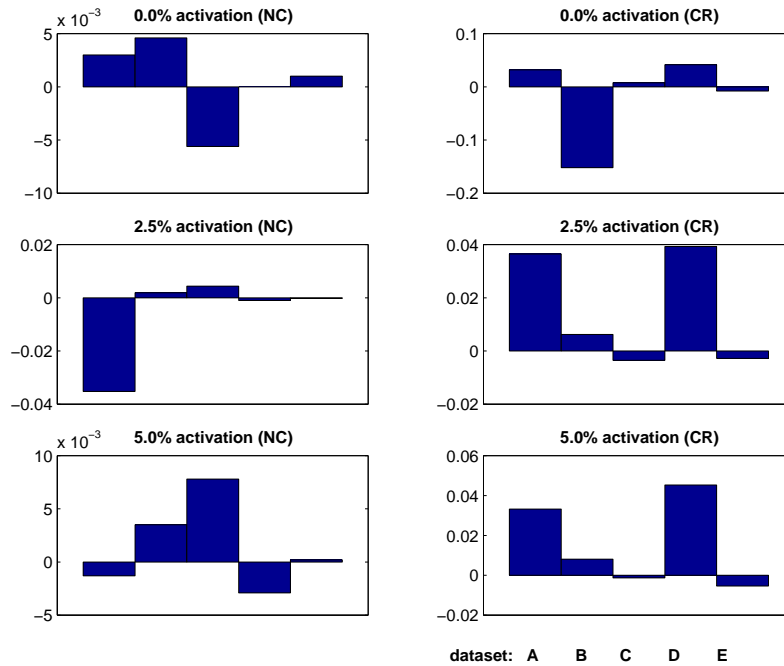


Figure 13: Median (over time) RMS (over space) error results (un-smoothed minus smoothed) for the MCFLIRT scheme applied to 5 synthetic data sets (A-E) exhibiting known motion at increasing intensities. A positive value indicates improved accuracy as a result of smoothing the cost function. Cost function notation corresponds to Table 1 and the results demonstrate the improvement in accuracy achieved by using the smoothed cost functions.

Overall, the smoothed cost functions outperform their un-smoothed versions.

4.3.3 Interpolation Scheme

To further improve the accuracy of the motion estimates, the next parameter we experimented with was the choice of interpolation scheme for the motion estimation. In addition to the standard tri-linear scheme, a windowed-sinc interpolation (using a Hanning window of size $7 \times 7 \times 7$) was tried. While considerably slower than trilinear interpolation, the sinc approach is able to further refine motion estimates after the initial trilinear stage has converged on a solution thus providing greater accuracy. The results in Figure 14 show the greater degree of accuracy achieved over using trilinear interpolation alone. Note that on the third data set (cropped to allow distinction between the

other four sets), the improvement was consistently over a value of 2.0.

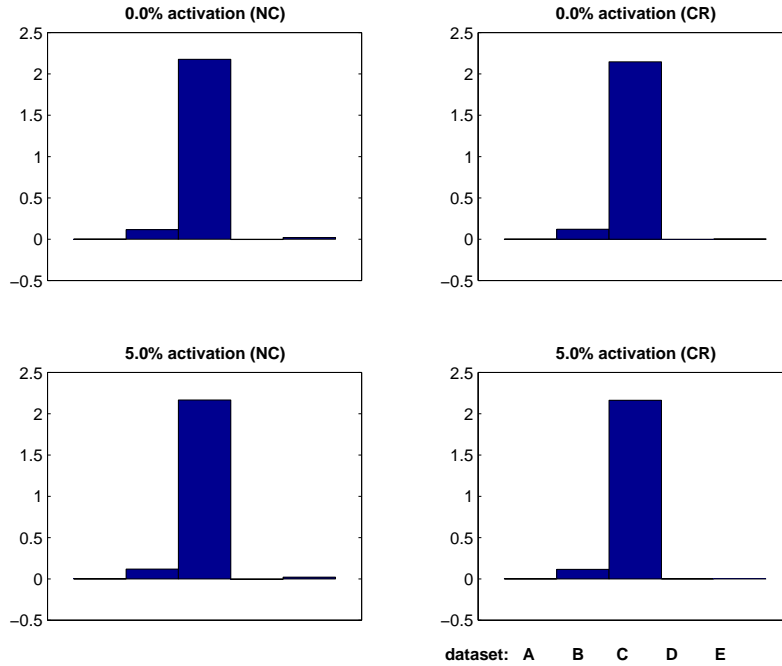


Figure 14: Median (over time) RMS (over space) error results for the MCFLIRT scheme applied to synthetic data exhibiting known motion of one of five designs and audiovisual activation at increasing intensities. A positive value indicates improved accuracy as a result of incorporating the final sinc interpolation stage. Cost function notation corresponds to Table 1 and demonstrates the improvement in accuracy achieved by using smoothed cost functions and additional sinc interpolation when compared to the basic trilinear scheme reported in Figure 13

4.3.4 Choice of Template Image

In an attempt to increase the accuracy of the scheme and as a final parameter investigation, a method using a mean image template was implemented. This scheme generates a mean image for the series by averaging all the volumes over time after the first three stages of trilinear interpolation-based motion correction have been carried out. In doing so we hope to be registering all volumes to a more generalised target which exhibits less overall variation from each volume in the series than the original target (middle) volume previously used. This new mean image is a robust target to which the original time series is then registered, again using three trilinear interpolation stages and an optional final sinc interpolation stage.

Because we are registering to a mean image, we no longer have “gold standard” values for the transformations found by the correction scheme. Therefore, to quantify the accuracy of the correction, a median absolute residual variation (MARV) score was created by initially de-meaning each voxel time-series and then measuring the median value of the residual absolute values in this time-series. That is,

$$MARV(x, y, z) = \sum_{t=1}^N |I_t(x, y, z) - I_{mean}(x, y, z)|/N.$$

This produce a volume of MARV scores for each voxel and the median of these values (over the volume) is then taken as a summary measure. This is effectively a measure characterising the level of inter-volume intensity variation (presumed to be due to subject motion) after retrospective motion correction has been applied. While this can only work for activation-free data (so that in perfect alignment the variance should be at minimum) it can give us a clear impression of the accuracy of the motion correction scheme. Because SPM rejects information outside a mask obtained from the data (end slice effects), the corrected median images were masked according to the corrected SPM data so that the measure reflected a consistent comparison across the schemes. The results shown in Figure 15 correspond to the MARV values generated after running MCFLIRT and SPM on the null-activation data set for both the low and severe motion designs.

Results using the RMS measure (Table 3) revealed that, although all three schemes provide sub-voxel accuracy, AIR 3.08 using Least Squares (which we found to give better results than the standard AIR measure) and Windowed Sinc interpolation was almost an order of magnitude worse than basic 3 stage tri-linear MCFLIRT. Accordingly we decided not to compare it further. However, we note that AIR was primarily designed to solve several different registration problems that arise in tomographic data sets [18] rather than optimised for FMRI motion correction.

From these results we conclude that for some cases (generally the low motion data), MCFLIRT with the Correlation Ratio cost function produces significantly smaller errors than SPM99 whilst in other cases (some of the high motion data) both methods give similar results. This can be seen by comparing the heights (MARV values) of the SPM bars with the CR bars (typically the best MCFLIRT cost function) where a 30% to 40% reduction can be seen in the first, second and fourth cases.

Slightly surprisingly we found that the use of a mean image template gave no discernable improvement in accuracy. We conclude that for artificial data where the motion is purely rigid, there is no advantage to using a (possibly blurred) average image over an image from the original data. We would expect that the mean template

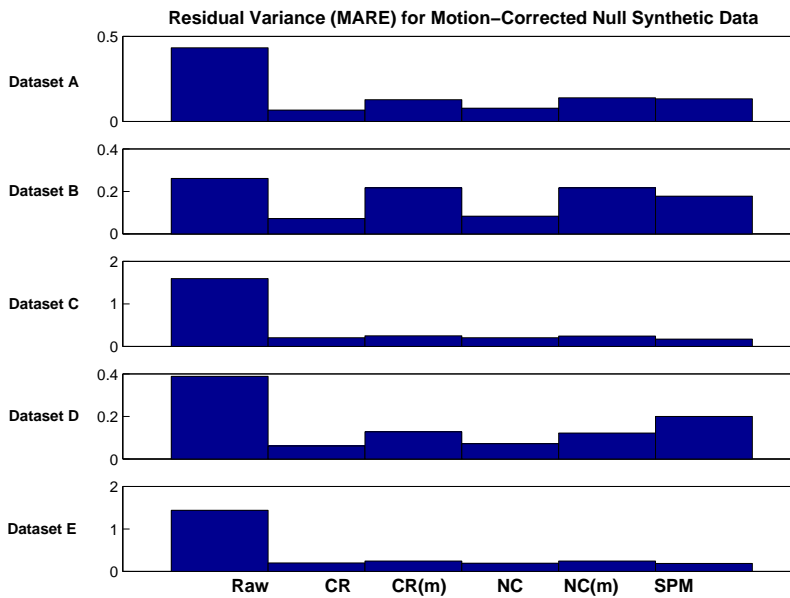


Figure 15: Median Absolute Residual Variation (MARV) values for corrected data processed by different motion correction schemes: Uncorrected, MCFLIRT w. CR, MCFLIRT w. NC, MCFLIRT w. CR & mean, MCFLIRT w. NC & mean, SPM99 run at full quality, with sinc interpolation and interpolation error adjustment

scheme could yield greater accuracy where the data includes some physical motion-induced artefacts and the choice of a reference image from the original dataset is not so obvious.

4.3.5 Null Data Study

Having established the accuracy of MCFLIRT on artificial data, we ran both our scheme and SPM99 on a number of real fMRI studies. In all instances, the subjects had been exposed to no stimulus (null data). The underlying assumption was that after motion correction on a null data study, we would expect the overall variation of the data to be lower than before correction as subject motion-induced variability had been minimized. Again, results were masked according to the SPM data to give a fair comparison.

Results, given in Figure 16, show considerable changes induced by SPM (both beneficial and detrimental) but only minimal changes induced by MCFLIRT. This is due to the fact that the amount of actual motion that occurred in these studies is very low, so that the changes in intensity in each voxel (as a result of motion correction) are also low — in fact lower than the expected changes induced by physiological processes. Consequently, these test results

are inconclusive since the test measure does not purely measure motion-induced changes but also physiological changes which dominate in this case. The only way one could expect to obtain quantitative analysis for real data would be to incorporate some form of position measurement into the scanner — a facility not available to us.

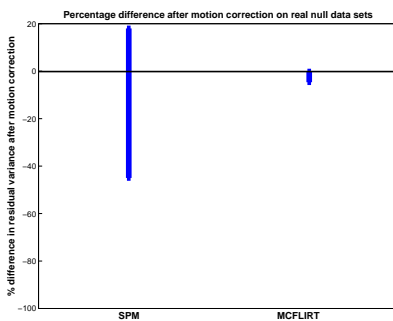


Figure 16: Summary MARV statistics for three sets of real data, comparing MCFLIRT w. CR, and SPM99 correction using full quality, sinc interpolation and interpolation error adjustment. The results show the range of percentage changes in residual variance as a result of the motion correction (i.e. comparing it to the uncorrected variance).

4.3.6 Real Activation Study

As we have described above, it is difficult to make accurate measurements pertaining to the accuracy of a motion correction scheme when presented with real data. With data exhibiting activation, examination of the time series after correction using an animation tool reveals no visible extreme affine movement although some motion artefacts remain. In particular, we are able to show good localisation of activations which would not be possible without motion correction first being carried out. The thresholded statistical maps shown in Figure 17 correspond to a 180 volume audio-visual experiment. Analysis was carried out using FEAT, FMRIBs Easy Analysis Tool using an Improved Linear Model [20]. In order to test the effectiveness of MCFLIRT on real data, the subject was asked to move his head during the experiment.

It can be seen, by comparing the activations from the uncorrected and corrected data sets, that in the uncorrected set a large number of false positives exist in both visual and auditory results. While it can be argued that both data sets are highly corrupted by this large motion (indeed even the corrected data set still exhibits some visible movement, albeit at a significantly smaller scale than the uncorrected data), the MCFLIRT-corrected visual stimulus

is well localised and allows an otherwise corrupted set of experimental data to yield potentially useful results.

5 Discussion

This paper has examined the problem of optimisation for fully automatic registration of brain images. In particular, the problem of avoiding local minima is addressed in two ways. Firstly, a general apodization (smoothing) method was formulated for cost functions in order to eliminate small discontinuities formed by discontinuous changes of the number of voxels in the overlapping field of view with changing transformation parameters. Secondly, a novel hybrid global-local optimisation method was proposed which uses prior knowledge about the problem (size of the brain, expected changes in scalings, *etc.*) while combining the speed of local optimisation with an initial search phase and multi-start optimisation component. The latter two components are similar to those used in Simulated Annealing and Genetic Algorithms — two popular, but slow, global optimisation techniques.

Only affine (linear) registration was examined in this paper as, although this is a much easier problem than general non-linear registration, finding the global minimum is still difficult. Furthermore, many non-linear methods rely on an initial affine registration to find a good starting position, and so having a good method of affine registration is important.

The global optimisation method proposed here does not, however, guarantee finding the global minimum. This is typical though, as even methods such as Simulated Annealing and Genetic Algorithms only provide a statistical guarantee which cannot be met in practice. The results, though, are encouraging, and by using finer search grids, the likelihood of finding the global minimum can be increased. This requires that there be sufficient time at hand, or a sufficiently fast computer. However, even with modest resources this method can find the global minimum and solve the registration problem within one hour (and often much less) more reliably than the other methods tested.

Optimisation is only one aspect of the registration problem, although it is practically a very important one. Other aspects such as interpolation, alternative cost functions and understanding the properties of existing cost functions remain important areas for further work. In addition, a theoretical justification for the current method and finding a method suitable for higher dimensional transformations are important areas for future research.

The implementations of the registration and motion correction methods (FLIRT and MCFLIRT) were tested using experiments designed to demonstrate the improved robustness and accuracy. These issues are important and

each is examined separately.

5.1 Robustness Study

Quantitative results for robustness of FLIRT were ascertained using a consistency test. This test is designed to examine the robustness of a registration method by comparing registrations obtained using various different, but known, initial starting positions of a given image. Results showed that the method was highly consistent on a set of difficult images. Furthermore, several other available packages were tested on the same set of images and did not achieve the same level of consistency, sometimes demonstrating substantial inconsistencies. These tests (together with those presented in [12]) showed that the robustness was due to the optimisation method, not just the choice of cost function, and that in order to achieve the robust registrations, multi-resolution local optimisation alone is insufficient. Moreover, the newly proposed hybrid local-global optimisation method achieves a much greater degree of robustness, which is necessary for fully automatic use, within a prescribed time-limit (less than one hour on a PC; e.g. registering two $1 \times 1 \times 1$ mm images typically takes 15 minutes on a 500MHz Pentium III).

5.2 Accuracy Study

In the case of accuracy we have shown that MCFLIRT optimisation routines, cost functions and sinc interpolation consistently achieve high levels of accuracy. In particular, the RMS test measure shows that the error is typically around 0.1mm which is more than an order of magnitude less than the voxel size of 4mm, but necessary to ensure subsequent statistical analysis is valid. Furthermore, tests demonstrated that the average performance of the MCFLIRT scheme was superior to both SPM99 and AIR v3.08. Results of the tests using real data that contained activation, where the underlying “ground truth” was not known and the RMS measure could not be used, were inconclusive due to the presence of (an unknown amount of) physiologically induced intensity variations. Note that in all cases (for the robustness and accuracy studies) the data sets used for comparative testing were independent of those used to tune the empirical parameters of the methods used.

Early tests using synthetic data have revealed that in cases where the motion is moderate (up to 2mm translation and 2° rotation), the sequential initialisation (see Figure 6) scheme yields an improvement in the accuracy of motion estimates compared to one where no sequential initialisation is performed. Conversely, in cases where the amplitude

of motion parameters were known to be high, there was no inherent disadvantage in making the assumption of an underlying smooth motion trend across timepoints.

We would be interested to see how robustly the schemes perform over time-series of varying length. If at all significant, we might expect to see some impact on the MCFLIRT mean image registration scheme where a longer time-series might provide a more general and robust template image. At present there is no guaranteed advantage in using the mean template in addition to the standard correction schedule but one would expect it to play a more beneficial role in correcting extended time-series exhibiting moderate to low motion artefacts.

The methods and results shown here are all for whole brain data sets, although the algorithms have also been successfully adapted to work with data sets containing very few slices (or just single slices) by restricting the transformations to be two dimensional, as the optimisation and apodizing methods also apply for these two dimensional registrations. However, when general three dimensional registration is required for images containing few slices, other approaches need to be used, such as those employed by some of the other packages tested here (where no global search is involved).

Practical registration packages usually require the setting of certain parameter values. The methods introduced here also contain several configurable parameters such as image resolutions for the various optimisation stages. These values have been selected empirically, over a wide range of data sets, to be as robust as possible for general brain images. However, when dealing with particular data sets these general settings may not be optimal and so most methods allow these values to be changed, via configurable options. When using other packages for comparative studies we have tried to select the best general parameter values (by consulting the appropriate documentation) but recognise that further improvement upon these results could be possible by careful selection of parameters. The tuning of registration methods is, at present, an undesirable necessity in many situations, which prevents easy automation. By using more robust algorithms this tuning of parameter settings can hopefully be minimised or avoided entirely.

In summary, the FLIRT and MCFLIRT packages are highly robust and accurate, as has been demonstrated by the quantitative experiments and by qualitative feedback. These methods have now been used to satisfactorily solve thousands of registration problems, some using extremely different imaging modalities. The binary and source code distributions for the MCFLIRT and FLIRT packages are available for downloading from www.fmrib.ox.ac.uk/fs1.

6 Acknowledgements

The authors wish to thank the Medical Research Council, the European MICRODAB project and the Engineering and Physical Sciences Research Council for supporting this work.

References

- [1] Bahrat B Biswal and James S Hyde. Contour-based registration technique to differentiate between task-activated and head motion-induced signal variations in fMRI. *Magnetic Resonance in Medicine*, 38:470–476, 1997.
- [2] P. Cachier and D. Rey. Symmetrization of the non-rigid registration problem using inversion-invariant energies: Application to multiple sclerosis. In *Medical Image Computing and Computer-Assisted Intervention*, pages 472–481, 2000.
- [3] D.L. Collins, P. Neelin, T.M. Peters, and A.C. Evans. Automatic 3D intersubject registration of MR volumetric data in standardized Talairach space. *Journal of Computer Assisted Tomography*, 18(2):192–205, 1994.
- [4] D. Vandermeulen F. Maes and P. Suetens. Comparative evaluation of multiresolution optimization strategies for multimodality image registration by maximization of mutual information. *Medical Image Analysis*, 3(4):373–386, 1999.
- [5] L. Freire and J.-F. Mangin. Motion correction algorithms of the brain mapping community create spurious functional activations. In M.F. Insana and R.M. Leahy, editors, *17th Int. Conf. on Information Processing in Medical Imaging*, pages 246–258. Springer, June 2001.
- [6] K.J. Friston, J. Ashburner, C.D. Frith, J.-B. Poline, J.D. Heather, and R.S.J. Frackowiak. Spatial registration and normalization of images. *Human Brain Mapping*, 2:165–189, 1995.
- [7] K.J. Friston, S.R. Williams, R. Howard, R.S.J. Frackowiak, and R. Turner. Movement-related effects in fMRI time-series. *Magnetic Resonance in Medicine*, 35:346–355, 1996.
- [8] J.V. Hajnal, N. Saeed, A. Oatridge, E.J. Williams, I.R. Young, and G.M. Bydder. Detection of subtle brain changes using subvoxel registration and subtraction of serial MR images. *Journal of Computer Assisted Tomography*, 19(5):677–691, 1995.

- [9] J.V. Hajnal, N. Saeed, E.J. Soar, A. Oatridge, I.R. Young, and G.M. Bydder. A registration and interpolation procedure for subvoxel matching of serially acquired MR images. *Journal of Computer Assisted Tomography*, 19(2):289–296, 1995.
- [10] Alan Julian Izenman. Recent developments in nonparametric density estimation. *Journal of the American Statistical Association*, 86(413):205–224, 1991.
- [11] M. Jenkinson. Measuring transformation error by RMS deviation. Internal Technical Report TR99MJ1, Oxford Centre for Functional Magnetic Resonance Imaging of the Brain, Department of Clinical Neurology, Oxford University, Oxford, UK, 1999. Available at www.fmrib.ox.ac.uk/analysis/techrep for downloading.
- [12] M. Jenkinson and S.M. Smith. A global optimisation method for robust affine registration of brain images. *Medical Image Analysis*, 5(2):143–156, June 2001.
- [13] F. Maes, A. Collignon, D. Vandermeulen, G. Marchal, and P. Suetens. Multimodality image registration by maximisation of mutual information. *IEEE Trans. on Medical Imaging*, 16(2):187–198, 1997.
- [14] J.B.A. Maintz and M.A. Viergever. A survey of medical image registration. *Medical Image Analysis*, 2(1):1–36, 1998.
- [15] W.H. Press, S.A. Teukolsky, W.T. Vetterling, and B.P. Flannery. *Numerical Recipes in C*. Cambridge University Press, second edition, 1995.
- [16] C. Studholme, D.L.G. Hill, and D.J. Hawkes. Automated 3D registration of MR and CT images of the head. *Medical Image Analysis*, 1(2):163–175, 1996.
- [17] J. West et al. Comparison and evaluation of retrospective intermodality brain image registration techniques. *Journal of Computer Assisted Tomography*, 21(4):554–566, 1997.
- [18] Roger P Woods. Automated Image Registration. Web page, April 1998. <http://www.bishopw.loni.ucla.edu/AIR3/>.
- [19] R.P. Woods, J.C. Mazziotta, and S.R. Cherry. MRI–PET registration with automated algorithm. *Journal of Computer Assisted Tomography*, 17(4):536–546, 1993.

- [20] M.W. Woolrich, B.D. Ripley, J.M. Brady, and S.M. Smith. Temporal autocorrelation in univariate linear modelling of fMRI data. *NeuroImage*, 14(6):1370–1386, 2001.

CostFunction	Definition	Minimum	Maximum
C^{LS}	$\sum(Y - X)^2$	0	∞
C^{NC}	$\frac{\sum(X.Y)}{\sqrt{\sum X^2}\sqrt{\sum Y^2}}$	-1	1
C^W	$\sum_k \frac{n_k}{N} \frac{\sqrt{\text{Var}(Y_k)}}{\mu(Y_k)}$	0	∞
C^{CR}	$\frac{1}{\text{Var}(Y)} \sum_k \frac{n_k}{N} \text{Var}(Y_k)$	0	1
C^{MI}	$H(X, Y) - H(X) - H(Y)$	$-\infty$	0
C^{NMI}	$\frac{H(X, Y)}{H(X) + H(Y)}$	0	1

Table 1: Mathematical definitions of the most commonly used intensity-based cost functions: Least Squares (LS); Normalised Correlation (NC); Woods (W); Correlation Ratio (CR); Mutual Information (MI); and Normalised Mutual Information (NMI). The notation is: quantities X and Y denote images, each represented as a set of intensities; $\mu(A)$ is the mean of set A ; $\text{Var}(A)$ is the variance of the set A ; Y_k is the k th iso-set defined as the set of intensities in image Y at positions where the intensity in X is in the k th intensity bin; n_k is the number of elements in the set Y_k such that $N = \sum_k n_k$; $H(X, Y) = -\sum_{ij} p_{ij} \log p_{ij}$ is the standard entropy definition where p_{ij} represents the probability estimated using the (i, j) joint histogram bin, and similarly for the marginals, $H(X)$ and $H(Y)$. Note that the sums in the first two rows are taken over all corresponding voxels.

Cost	# sets most accurate	# sets 2nd most accurate
Normalized Correlation	8	5
Correlation Ratio	2	7
Mutual Information	2	1
Normalized Mutual Information	0	2
Least Squares	3	0

Table 2: Accuracy counts for the five cost functions offered by MCFLIRT

	Uncorrected	AIR	SPM	MCFLIRT
Sum of squared intensity errors	936.5866	406.8876	1.6405	1.5171
RMS error (mm)	2.3360	1.7570	0.1064	0.1102

Table 3: RMS deviation values for synthetic null data

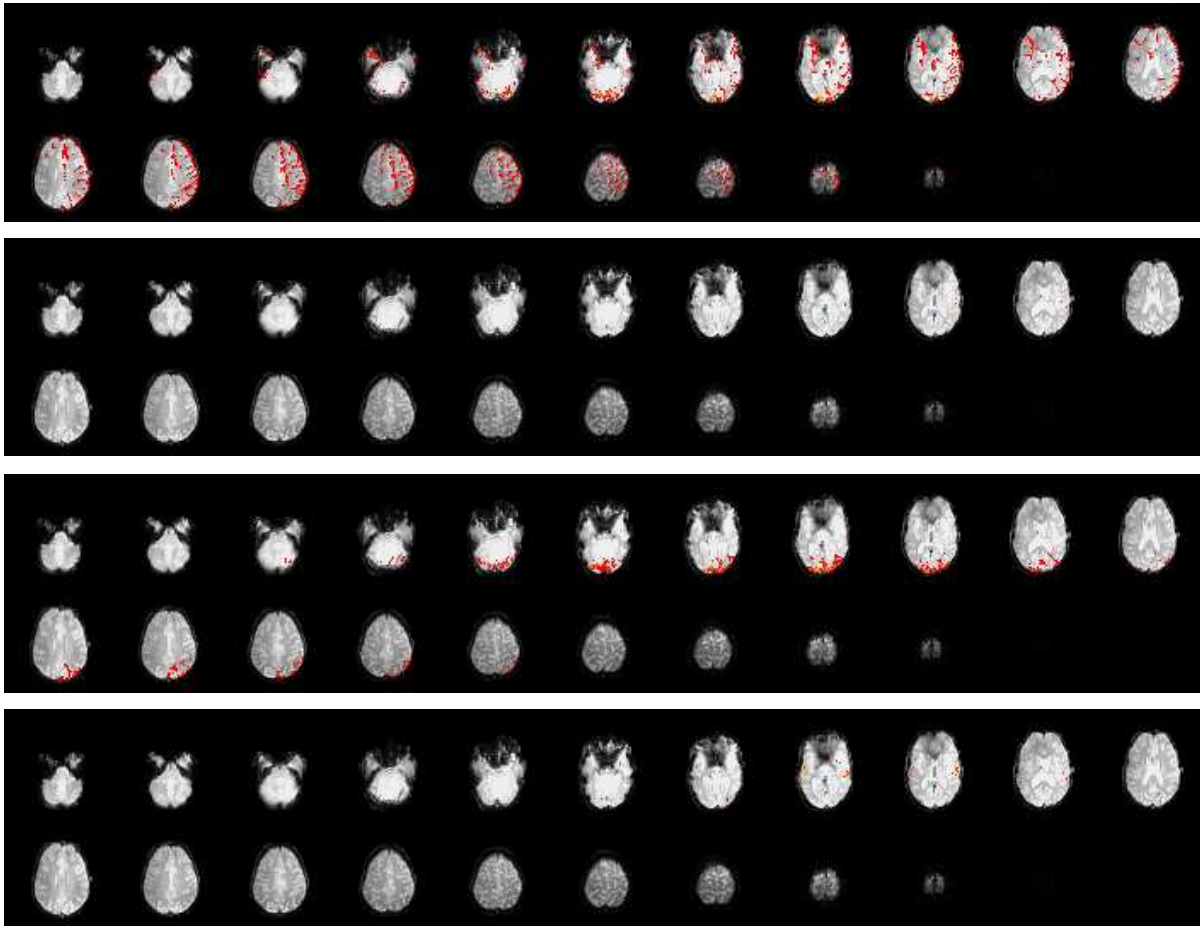


Figure 17: The resulting thresholded z-statistics from a FEAT analysis of real audiovisual data (Auditory 45s OFF, 45s ON and visual 30s OFF, 30s ON) which has been motion corrected. Prior to motion correction, the series exhibited a large degree of motion as the subject had been requested to move as much as possible during the experiment. Maps are: (from top) Visual paradigm z-stats (uncorrected), auditory z-stats (uncorrected), visual z-stats (MCFLIRT), auditory z-stats (MCFLIRT)